Available online at www.sciencedirect.com
ScienceDirect
Trans. Nonferrous Met. Soc. China 22(2012) 2541−2547
Transactions of Nonferrous Metals Society of China
www.tnmsc.cn

Synthesis of spinel $LiMn_2O_4$ microspheres with durable high rate capability

ZHOU Yu-bo[1, 3], DENG Yuan-fu[2, 3], YUAN Wei-hao[2], SHI Zhi-cong[3], CHEN Guo-hua[3]

1. School of Environmental Science and Technology, Dalian University of Technology, Dalian 116024, China;
2. The Key Laboratory of Fuel Cell Technology of Guangdong Province,
School of Chemistry and Chemical Engineering, South China University of Technology, Guangzhou 510640, China;
3. Centre for Green Products and Processing Technologies,
Guangzhou HKUST Fok Ying Tung Research Institute, Guangzhou 511458, China

Received 9 July 2012; accepted 19 August 2012

Abstract: Spinel $LiMn_2O_4$ microspheres with durable high rate capability were synthesized by a facile route using spherical $MnCO_3$ precursors as the self-supported templates, combined with the calcinations of $LiNO_3$ at 700 °C for 8 h. The spherical $MnCO_3$ precursors were obtained from the control of the crystallizing process of Mn^{2+} ions and NH_4HCO_3 in aqueous solution. The effects of the mole ratio of the raw materials, reaction time, and reaction temperature on the morphology and yield of the $MnCO_3$ were investigated. The as-synthesized $MnCO_3$ and $LiMn_2O_4$ microspheres were characterized by powder X-ray diffractometry (XRD) and scanning electron microscopy (SEM). Galvanostatic charge/discharge tests indicate that the spinel $LiMn_2O_4$ microspheres deliver a discharge capacity of 90 mA·h/g at 10*C* rate show good capacity retention capability (75% of their initial capacity after 800 cycles at 10*C* rate). The durable high rate capability suggests that the as-synthesized $LiMn_2O_4$ microspheres are promising cathode materials for high power lithium ion batteries.

Key words: $MnCO_3$ microspheres; self-supported template; $LiMn_2O_4$ microspheres; rate capability

1 Introduction

Lithium ion batteries (LIBs) have become revolutionized portable electronic devices in the past two decades [1]. They are also expected to make a great impact on the pure electric vehicles (EV) and hybrid electric vehicles (HEV) [2]. The battery performance depends critically on the materials, and therefore the development of new materials is important for advancing battery technology. The current commercial lithium ion batteries commonly based on the layered cobalt oxides cathode materials can hardly fulfill the requirement of high power applications such as HEV and EV [3]. Thus, the novel cathode materials with high energy and power density have received considerable interest [4−6]. Spinel $LiMn_2O_4$ is a prospective candidate for the cathode material for EV and HEV because of its intrinsic advantages of suitable Mn^{4+}/Mn^{3+} redox potential (4.0 V, vs Li^+/Li), low cost, high abundance, better safety, and environmental compatibility. Especially, the three-dimensional lithium ion channels of the three-dimensional crystal structure $LiMn_2O_4$ is beneficial for the intercalation and deintercalation of lithium ion at high rate [7]. However, the application of spinel $LiMn_2O_4$ materials is hampered by the problem of capacity decay during cycling, which mainly results from Mn dissolution via a disproportionation reaction ($2Mn^{3+}\rightarrow Mn^{2+}+Mn^{4+}$) and structural transformation from cubic to tetragonal phase that is induced by Jahn– Teller distortion of Mn(III) with high spin [8]. Previous studies demonstrated that the discharge capacities, cycling life, and rate performance of rechargeable lithium ion batteries are dramatically affected by the particle size, surface morphology and synthesized method of the active materials [9]. It is commonly acknowledged that the nanostructured electrode materials can overcome the limits, especially the power density. Various nanostructured $LiMn_2O_4$, such as nanoparticles [10], mesoporous materials [11], double-shelled hollow microspheres [12], and one-dimensional (1-D) nanomaterials (nanowires [13], nanorods [3] and nanotube [14]) have

Foundation item: Project (2011M501090) supported by the China Postdoctoral Science Foundation; Project (SCUT2012ZZ0042) supported by the Fundamental Research Funds for the Central Universities; Project supported by the "SPR−2011"of South China University of Technology; Project (NRC07/08.EG01) supprted by the Fok Ying Tung Foundation
Corresponding author: DENG Yuan-fu; Tel: +86-20-87112053; Fax: +86-20-34685679; E-mail: chyfdeng@scut.edu.cn
DOI: 10.1016/S1003-6326(11)61498-2

been investigated aiming at the application in high-power LIBs. Although nanometer- sized $LiMn_2O_4$ has demonstrated improvement in rate capability, its tap density is very low compared with that of the conventional oxide electrode material. Low tap density results in low volumetric energy density, and consequently, nano-$LiMn_2O_4$ cathodes are not suitable for lithium-ion batteries designed for applications in plug-in hybrid vehicles (PHEVs) or electric vehicles. In addition, the electrodes prepared with nano-scaled cathode materials turn out to be easily loosened and slough off, which results in bad cycleability of the electrode. Therefore, it is of great importance, to develop a facile and scalable method to synthesize the electrode materials with spherical morphology (high tap-density) and reasonable and uniform size distribution (high rate performance).

Herein, the preparation of $LiMn_2O_4$ microspheres using spherical $MnCO_3$ precursors was reported, which were obtained from the control of the crystallizing process of Mn^{2+} ions and NH_4HCO_3 in aqueous solution, as the self-supporting templates. Without surface coating or cation doping, the as-prepared $LiMn_2O_4$ microspheres could deliver good durability at high charge/discharge rates after 800 cycles.

2 Experimental

2.1 Synthesis

2.1.1 Synthesis of spherical $MnCO_3$

The synthesis of spherical $MnCO_3$ was carried out by controlling the crystallizing process of the following reaction equation in aqueous solution.

$$MnCl_2{\cdot}4H_2O+2NH_4HCO_3 \longrightarrow MnCO_3\downarrow+2NH_4Cl+CO_2\uparrow+5H_2O \quad (1)$$

In a typical experiment, NH_4HCO_3 (2.752 g, 40 mmol) was dissolved in 50 mL deionized water and added to 10 mL solution containing 3.444 g $MnCl_2{\cdot}4H_2O$. After being stirred at 35 °C for 20 min, some pale yellow powders were precipitated from the reaction solution. After filtration, the pale yellow powders were washed with distilled water and ethanol three times and dried at 80 °C in vacuum. In addition, the effects of the mole ratio of the raw materials, reaction time, reaction temperature and surfactant on the morphology and yield of the $MnCO_3$ were investigated.

2.1.2 Synthesis of $LiMn_2O_4$ microspheres

The $LiMn_2O_4$ microspheres were prepared according to the following equation:

$$MnCO_3+LiNO_3 \longrightarrow LiMn_2O_4+N_xO_y\uparrow \quad (2)$$

In a typical experiment, the obtained spherical $MnCO_3$ powders were mixed with $LiNO_3$ in stoichiometric ratio of 2.00:1.05, and then the mixture was ground to obtain a homogeneous mixture. After that, the homogeneous mixture was calcined at 700 °C for 8 h to obtain black $LiMn_2O_4$ microspheres.

2.2 Characterization

The structures and morphologies of the as-prepared materials were characterized by powder X-ray diffractometry (XRD, Bruker D8 Advance powder diffractometer) using Cu K_α radiation at 40 kV, 40 mA and steps of 0.020 and field emission scanning electron microscopy (SEM, Jeol JSM—6390).

The electrochemical characterizations of the sample were performed using CR2025 coin-type cell. The electrode was prepared by mixing the as-prepared active material (80%, mass fraction), acetylene black (10%) and polyvinylidene fluoride (PVDF) binder (10%) with a mass ratio of 8:1:1. After these materials were thoroughly mixed in N-methyl-2-pyrrolidone (NMP) solution, the prepared slurry was coated on Al foil in the N-methyl pyrrolidinone (NMP). The slurry was coated on an aluminum foil and dried at 90 °C for 2 h in a vacuum oven. The electrode was incorporated into the coin cell with a lithium foil anode and a Celgard 2325 microporous membrane separator in a dry glove box under argon. The electrolyte used was 1.0 mol/L $LiPF_6$ ethylene carbonate (EC) solution and ethyl methyl carbonate (EMC) (3:7 in volume). The electrochemical charge-discharge measurements were carried out in the voltage range from 3.2 to 4.4 V (vs Li^+/Li) at different rates.

3 Results and discussion

3.1 Effect of reaction temperature on $MnCO_3$ yield and morphology

Table 1 shows the yield of $MnCO_3$ obtained at different reaction temperatures (35, 45 and 55 °C) when the reactions were kept in aqueous solution with the mixture of $MnCl_2{\cdot}4H_2O$ and NH_4HCO_3 at a mole ratio of 1:2. The reaction time was 20 min.

Table 1 Yield of $MnCO_3$ at different reaction temperatures

Temperature/°C	Yield ratio/%	Morphology
35	99.70	Uniform sphere
45	99.45	Square
55	98.40	Square

The above results clearly reveal that a little high yield of $MnCO_3$ can be obtained at 35 °C, which probably can be attributed to the fast decomposition of NH_4HCO_3 at a high temperature. Figure 1 shows the typical morphologies of the $MnCO_3$ obtained at different temperatures. As seen in Fig. 1(a), the $MnCO_3$ precursors obtained at 35 °C are uniform spheres with average

diameters of around 1 μm. However, the SEM images of $MnCO_3$ prepared at 45 and 55 °C (Figs. 1(b) and 1(c)) show square structure and some agglomeration. Thus, 35 °C was selected as the optimum temperature for the synthesis of $MnCO_3$ microspheres.

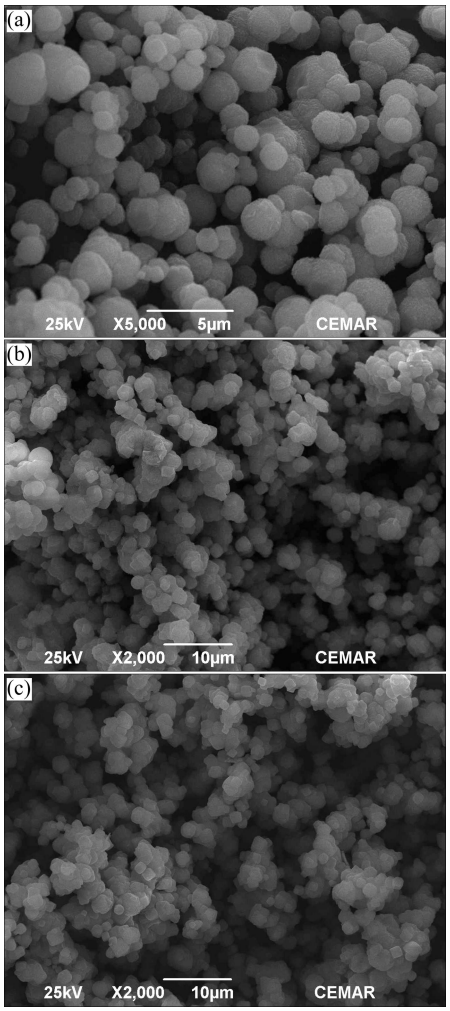

Fig. 1 SEM images of $MnCO_3$ obtained at different reaction temperatures: (a) 35 °C; (b) 45 °C; (c) 55 °C

3.2 Effect of reaction time on $MnCO_3$ yield and morphology

When the reaction was kept at 35 °C, the effect of reaction time on the $MnCO_3$ yields was investigated. As shown in Table 2, the $MnCO_3$ yields were all above 99% with no obvious difference when the reactions were kept at different reaction time. Because of some disadvantages including time consumption, energy wastage and some agglomeration of the obtained products, we selected 20 min as the most suitable condition for the synthesis of $MnCO_3$. Figure 2 shows the morphology of the $MnCO_3$ obtained for different reaction times.

Table 2 Yield of $MnCO_3$ obtained at 35 °C for different reaction times

Reaction time/min	Yield ratio/%	Morphology
20	99.45	Uniform sphere
40	99.00	Agglomeration
60	99.90	Agglomeration

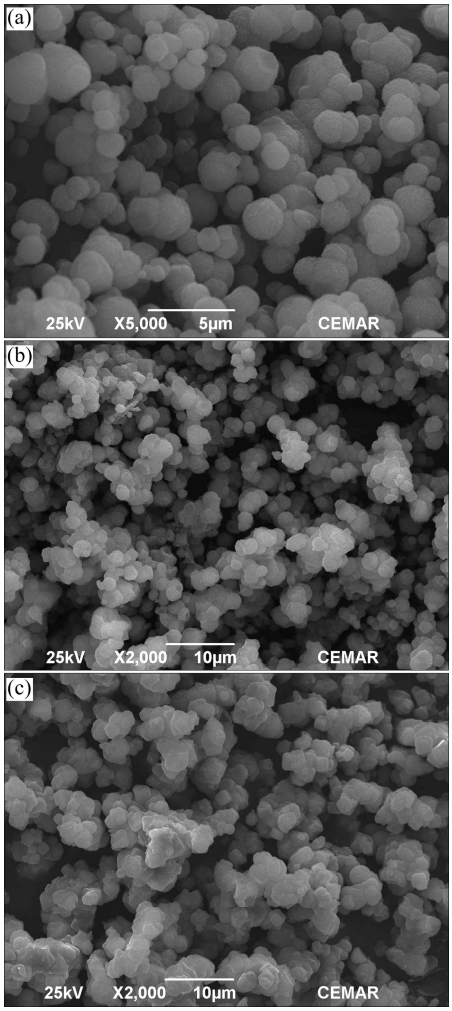

Fig. 2 SEM images of $MnCO_3$ obtained at 35 °C for different reaction times: (a) 20 min; (b) 40 min; (c) 60 min

3.3 Effect of ratio of $MnCl{\cdot}4H_2O$ and NH_4HCO_3 on $MnCO_3$ yield and morphology

Table 3 lists the yield of $MnCO_3$ at different ratios of $MnCl{\cdot}4H_2O$ to NH_4HCO_3. The experiments were conducted at 35 °C for 20 min. The results reveal that the yield of the $MnCO_3$ increases with the increase of the mole ratio of $MnCl{\cdot}4H_2O$ to NH_4HCO_3. When the ratio is 1:1, the yield of $MnCO_3$ is only 45.75%. When the ratio is 1:2, the yield is nearly up to 100%. These results can be explained by the fact that the chemical equilibrium moves right if the concentration of reactants increases. However, when the ratio increases to 1:5, the yield is only 94.25%, which is probably attributed to the side reactions in the high pH value solution by the addition of surplus NH_4HCO_3. Combining with the

Table 3 Yield and morphology of $MnCO_3$ at different mole ratios of $MnCl·4H_2O$ to NH_4HCO_3

Mole ratio	Yield ratio/%	Morphology
1:1	45.75	Uniform square
1:2	98.90	Uniform sphere
1:3	99.90	Agglomeration particle
1:5	94.25	Agglomeration particle

decrease of cost and the increase of purity of products, the ratio of 1:2 was selected as the optimal experimental condition.

Figure 3 shows the morphologies of the $MnCO_3$ obtained from different mole ratios of $MnCl·4H_2O$ to NH_4HCO_3. As shown in Fig. 3(a), the $MnCO_3$ prepared with the ratio of 1:1 shows the uniform squares with average diameters of around 1 μm. However, the $MnCO_3$ prepared at the ratios of 1:3 and 1:4 (Figs. 3(b) and 3(c)) clearly display to some degree agglomeration.

Based on the above observations, we selected the mole ratio of 1:2, temperature 35 °C and reaction time 20 min as the optimal parameters to obtain the $MnCO_3$ with good morphology and high yield.

3.4 Characterizations of $MnCO_3$ precursor and $LiMn_2O_4$ microspheres

Figure 4(a) shows the XRD pattern of the $MnCO_3$ obtained from the optimal experimental conditions. All the diffraction peaks are consistent with the standard card (JCPDS card 00-044-1472), which demonstrated that the as-synthesized $MnCO_3$ is with high purity and crystallinity.

Figure 4(b) displays the XRD pattern of the $LiMn_2O_4$ microspheres produced from the calcination of the mixture of $LiNO_3$ and spherical $MnCO_3$ precursors at 700 °C for 8 h. The diffraction peaks can be assigned to well-crystallized cubic spinel $LiMn_2O_4$ (JPSDS card 35-0782). The refinement cell parameter is 8.196 Å (calculated using the Jade Software), which is smaller than the standard value of 8.248 Å. This result demonstrates that the manganese ions in the octahedral sites are partially replaced by lithium ions in the spinel lattice [3].

Figure 5 shows the typical SEM image of the $LiMn_2O_4$ microspheres produced from the calcination of the mixture of $LiNO_3$ and spherical $MnCO_3$ precursors at 700 °C for 8 h. In Fig. 5, most of the obtained $LiMn_2O_4$ sample preserved the spherical morphology of the $MnCO_3$ precursor except for some aggregation because of the calcination at high temperature. In addition, some small particles were observed on the surface of the $LiMn_2O_4$ microspheres, which probably results from the gas evolution caused by the thermal decomposition of $MnCO_3$ and $LiNO_3$.

3.5 Electrochemical properties of $LiMn_2O_4$ microspheres

Figure 6 shows the typical galvanostatic charge-

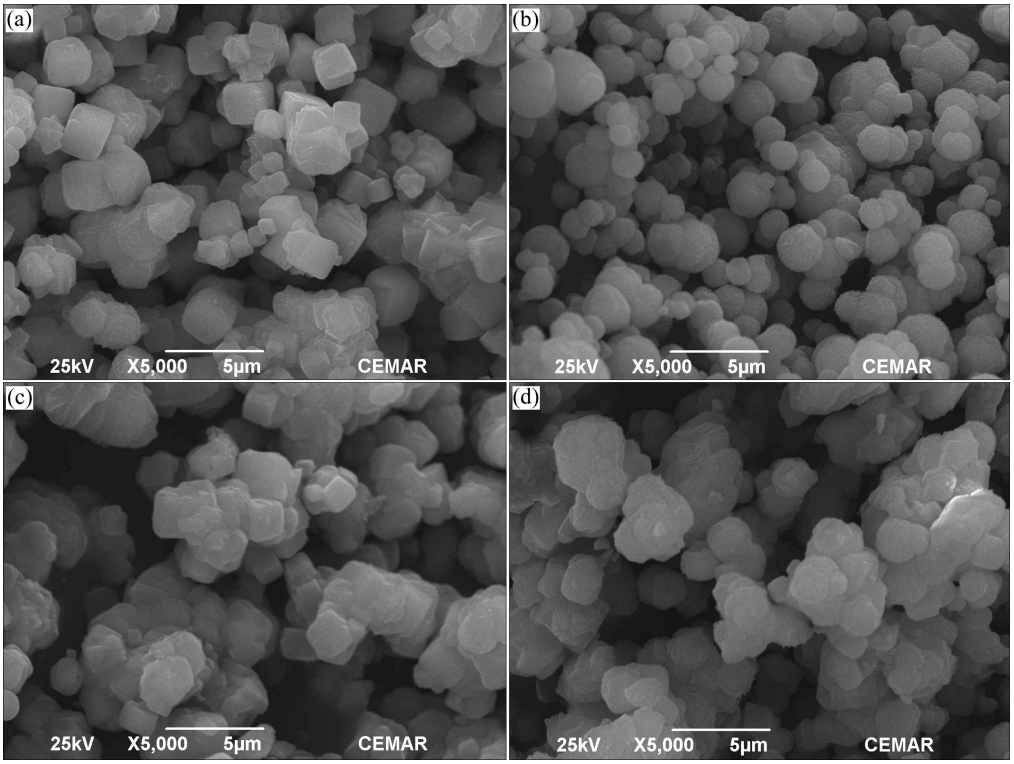

Fig. 3 SEM images of $MnCO_3$ obtained of different mole ratios of $MnCl·4H_2O$ to NH_4HCO_3: (a) 1:1; (b) 1:2; (c) 1:3; (d) 1:5

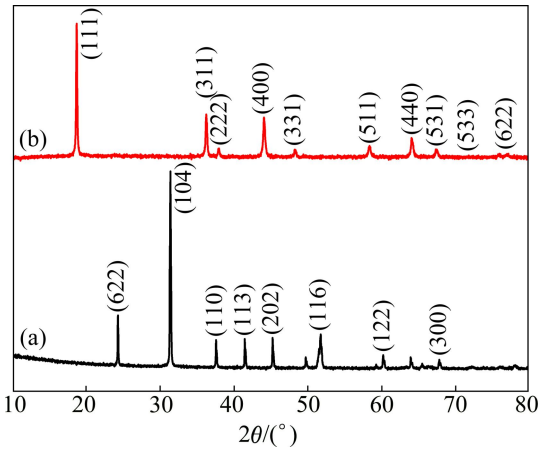

Fig. 4 XRD patterns of $MnCO_3$ obtained from optimal experimental condition (a) and $LiMn_2O_4$ microspheres produced from calcination of mixture of $LiNO_3$ and $MnCO_3$ (b)

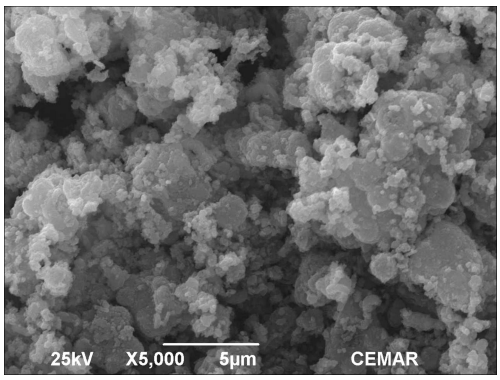

Fig. 5 SEM image of $LiMn_2O_4$ microspheres

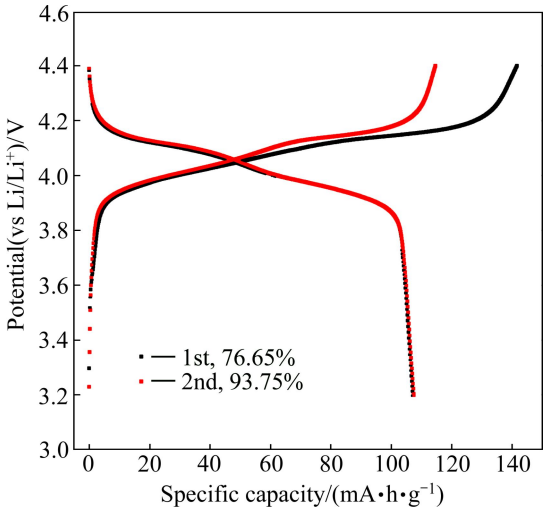

Fig. 6 Charge-discharge curves of $LiMn_2O_4$ microspheres at 0.1*C*

discharge profiles of $LiMn_2O_4$ microspheres tested at potential range of 3.2−4.4 V and current rate of 0.1*C*. Both of the charge and discharge curves exhibit two distinguishable pseudo plateaus, which are attributed to the two-phase transformation of λ-MnO_2/ $Li_{0.5}Mn_2O_4$ and $Li_{0.5}Mn_2O_4$/$LiMn_2O_4$ [14], respectively. The initial specific capacity is 109 mA·h/g at 0.1*C*, with a coulomb efficiency of 75.65%. Although the initial specific capacity of the as-synthesized material is lower than the most recently reported results [3, 9−14], the specific capacity of the as-synthesized material of 103.0 mA·h/g (as shown in Fig. 7) is comparable to some of the reported results [15−17]. Furthermore, the specific capacity of 96 mA·h/g and the retention capability of larger than 93% after 100 cycles at 1.0*C* of the $LiMn_2O_4$ microspheres demonstrate that they exhibit good cycling stability, which can be attributed to their reasonable particle size, stable spherical structure and small surface areas (0.6 m^2/g).

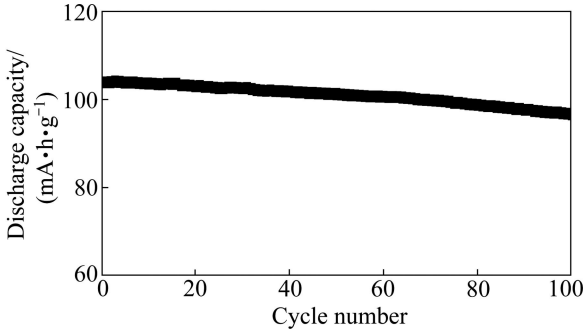

Fig. 7 Cycling performance of $LiMn_2O_4$ microspheres at 1.0*C* rate

To evaluate the high-power capability, the $LiMn_2O_4$ microspheres prepared at 700 °C were cycled at different discharge/charge current densities ranging from 1 to 20*C*. Figure 8 shows the discharge curves of the as-synthesized material at different discharge current densities. As anticipated, the profiles at low charge/discharge rates clearly show two distinguished plateaus located at about 4.1 and 4.0 V (vs Li/Li^+). When the charge/discharge rate is over 10*C*, the separation of the two discharge plateaus gradually becomes blurred and

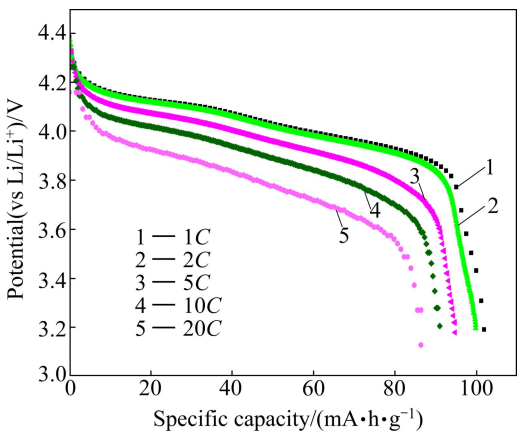

Fig. 8 Discharge curves of $LiMn_2O_4$ microspheres at different rates

the plateau voltages shift lower due to the increased cell polarization at very high current rates.

Figure 9 displays the rate performance of the electrode made from $LiMn_2O_4$ microspheres. As the current density increased from 1 to 20*C*, the discharge capacity decreased slightly from 103 to 86.4 mA·h/g. At a rate of 10*C*, a discharge capacity of 91 mA·h/g can be obtained. When the current density was decreased from 20 to 1*C*, the discharge capacity went back up to 101 mA·h/g, revealing the superior reversibility of the $LiMn_2O_4$ microspheres and their suitability as a high rate cathode material. In addition, the capacities remained at 68 mA·h/g even after 800 discharge/charge cycles at 10*C* (as shown in Fig. 10), and the corresponding capacity retentions were 75%. It is safe to say that the as-prepared $LiMn_2O_4$ microspheres exhibit good rate capability and cycleability.

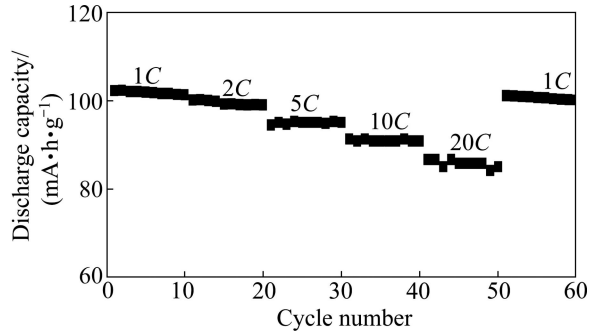

Fig. 9 Rate and cycling performance of $LiMn_2O_4$ microspheres

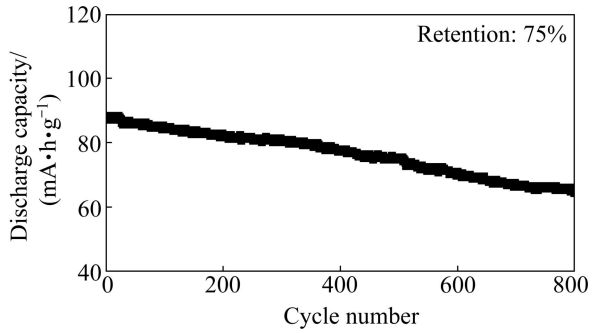

Fig. 10 Cycling performance of $LiMn_2O_4$ microspheres at 10*C* rate

4 Conclusions

1) Spinel $LiMn_2O_4$ microspheres with durable high rate capability were synthesized by a facile route using spherical $MnCO_3$ precursors as the self-supported templates, combined with the calcinations of $LiNO_3$ at 700 °C for 8 h.

2) The reactant ratio, reaction time and reaction temperature have significant effects on the morphology and yield of the $MnCO_3$ precursors.

3) The obtained $LiMn_2O_4$ microspheres exhibited remarkable high rate capability with 85 mA·h/g at 20*C* current density and durable capacity retention capability at 1.0 and 10*C* (the capacity retention capabilities are larger than 93% at 1.0*C* for 100 cycles and 75% at 10*C* for 800 cycles, respectively).

4) The excellent electrochemical properties are attributed to the reasonable particle size, stable spherical structure and small surface areas.

References

[1] JEONG G J, KIM Y U, KIM Y J, SOHN H J. Prospective materials and applications for Li secondary batteries [J]. Energy Environmental Science, 2011, 4(6): 1986−2002.

[2] TARSCON J M, RECHAM N, ARMAND M, CHOTARD J N, BARPANDDA P, WALKER W, DUPONT L. Hunting for better Li-based electrode materials via low temperature [J]. Chemistry of Materials, 2010, 22(3): 724−739.

[3] CHENG F Y, WANG H B, ZHU Z Q, WANG Y Y, ZHANG T R, TAO Z L, CHEN J. Porous $LiMn_2O_4$ nanorods with durable high-rate capability for rechargeable Li-ion batteries [J]. Energy Environmental Science, 2011, 4(9): 3668−3675.

[4] ELLIS B L, LEE K T, NAZARL F. Positive electrode materials for Li-ion and Li-batteries [J]. Chemistry of Materials, 2010, 22(3): 691−714.

[5] GAO X P, YANG H X. Multi-electron reaction materials for high energy density batteries [J]. Energy Environmental Science, 2010, 3(2): 174−189.

[6] COURTEL F M, DUNCAN H, ABU-LEBDEH Y, DAVIDSON I J. High capacity anode materials for Li-ion batteries based on spinel metal oxides AMn_2O_4 [J]. Journal of Materials Chemistry, 2011, 21(27): 10206−10218.

[7] LIU W, KOWAL K, FARRINGTON G C. Mechanism of the electrochemical insertion of lithium into $LiMn_2O_4$ spinels [J]. Journal of the Electrochemical Society, 1998, 145(2): 459−465.

[8] YANG X, TANG W, LIU Z, MAKITA Y, OOI K. Synthesis of lithium-rich $Li_xMn_2O_4$ spinels by lithiation and heat-treatment of defective spinels [J]. Journal of Materials Chemistry, 2002, 12(3): 489−495.

[9] WANG Z Y, ZHOU L, LOU X W. Metal oxide hollow structures are promising electrode materials [J]. Advanced Materials, 2012, 24(14): 1903−1911.

[10] OKUBOM, HOSONO E, KIM J, ENOMOTO M, KOJIMA N, KUDO T, ZHOU H S, HONMA I. Nanosize effect on high-rate Li-ion intercalation in $LiCoO_2$ electrode [J]. Journal of the American Chemical Society, 2007, 129 (23): 7444−7452.

[11] JIAO F, BAO J, HILL A H, BRUCE P G. Synthesis of ordered mesoporous Li−Mn−O spinel as a positive electrode for rechargeable lithium batteries [J]. Angewandte Chemie International Edition, 2008, 47: 9711−9716.

[12] DING Y L, ZHAO X B, XIE J, CAO G S, ZHU T J, YU H M, SUN C Y. Double-shelled hollow microspheres of $LiMn_2O_4$ for high-performance lithium ion batteries [J]. Journal of Materials Chemistry, 2011, 21(26): 9475−9479.

[13] LEE H W, MYRALIDHARAN P, RUFFO R, MARI C M, CUI Y, KIM D K. Ultrathin spinel $LiMn_2O_4$ nanowires as high power cathode materials for Li-ion batteries [J]. Nano Letters, 2010, 10(10): 3852−3856.

[14] DING Y L, XIE J, CAO G S, ZHU T J, YU H M, ZHAO X B. Single-crystalline $LiMn_2O_4$ nanotubes synthesized via template-

engaged reaction as cathodes for high-power lithium ion batteries [J]. Advanced Functional Materials, 2011, 21(2): 348−355.

[15] LUO J Y, XIONG H M, XIA Y Y. $LiMn_2O_4$ nanorods, nanothorn microspheres, and hollow nanospheres as enhanced cathode materials of lithium ion battery [J]. The Journal of Physical Chemistry C, 2008, 112(31): 12051−12057.

[16] YUE H J, HUANG X K, LV D P, YANG Y. Hydrothermal synthesis of $LiMn_2O_4$/C composite as a cathode for rechargeable lithium-ion battery with excellent rate capability [J]. Electrochimica Acta, 2009, 54: 5363−5367.

[17] AHN D, GIM J, SHIN N, KOOY M, KIM J, SHIN T J. Nanorod-assembled spinel $Li_{1.05}Mn_{1.95}O_4$ rods with a central tunnel along the rod-axis for high rate capability of rechargeable lithium-ion batteries [J]. Electrochimica Acta, 2010, 55: 8888−8893.

耐久型高倍率性能锰酸锂微球的合成

周玉波[1,3]，邓远富[2,3]，袁伟豪[2]，施志聪[3]，陈国华[3]

1. 大连理工大学 环境科学与工程学院，大连 116024；
2. 华南理工大学 化学与化工学院 广东省燃料电池技术重点实验室，广州 510640；
3. 广州市香港科大霍英东研究院，广州 511458

摘　要：以 Mn^{2+}和 NH_4HCO_3 为原料，通过控制结晶法合成球形 $MnCO_3$ 前驱体模板。以 $LiNO_3$ 和 $MnCO_3$ 为原料，按照一定的摩尔比机械混合，在 700 °C 下煅烧 8 h，合成高倍率性能和长循环性能的球形尖晶石 $LiMn_2O_4$ 材料。分别考查原料的摩尔比、反应时间以及反应温度对前驱体 $MnCO_3$ 形貌和产率的影响。采用 X 射线粉末衍射和扫描电镜对合成的 $MnCO_3$ 和 $LiMn_2O_4$ 进行表征，对 $LiMn_2O_4$ 样品进行室温条件下的充放电性能测试。电化学测试结果表明：尖晶石锰酸锂微球在 10*C* 的放电倍率下的首次放电容量达 90 mA·h/g (1*C* 放电容量为 148 mA/g)，800 次循环后容量保持率达到 75%。该方法合成的 $LiMn_2O_4$ 微球作为高功率型锂离子电池的正极材料有着较好的应用前景。

关键词：碳酸锰微球；模板法；锰酸锂微球；高倍率性能

(Edited by LONG Huai-zhong)